NMR Provides Checklist of Generic Properties for Atomic-Scale Models of Periodic Mesoporous Silicas

Ilja G. Shenderovich,*,†,‡ Daniel Mauder,† Dilek Akcakayiran,§ Gerd Buntkowsky,‖ Hans-Heinrich Limbach,*,† and Gerhard H. Findenegg§

Institut für Chemie und Biochemie, Freie Universität Berlin, Takustrasse 3, Berlin, D-14195, Germany, Institut für Chemie, Stranski-Laboratorium, Technische Universität Berlin, Strasse des 17. Juni 124, Berlin, D-10623, Germany, Institut für Physikalische Chemie, Universität Jena, Helmholtzweg 4, Jena, D-07743, Germany, and V. A. Fock Institute of Physics, St. Petersburg State University, Ulyanovskaja 1, 198504 Peterhof, Russia

Received: May 14, 2007; In Final Form: August 14, 2007

MCM-41 and SBA-15 silicas were studied by ^{29}Si solid-state NMR and ^{15}N NMR in the presence of ^{15}N-pyridine with the aim to formulate generic structural parameters that may be used as a checklist for atomic-scale structural models of this class of ordered mesoporous materials. High-quality MCM-41 silica constitutes quasi-ideal arrays of uniform-size pores with thin pore walls, while SBA-15 silica has thicker pore walls with framework and surface defects. The numbers of silanol (Q^3) and silicate (Q^4) groups were found to be in the ratio of about 1:3 for MCM-41 and about 1:4 for our SBA-15 materials. Combined with the earlier finding that the density of surface silanol groups is about three per nm^2 in MCM-41 (Shenderovich, et al. *J. Phys. Chem. B* **2003**, *107*, 11924) this allows us to discriminate between different atomic-scale models of these materials. Neither tridymite nor edingtonite meet both of these requirements. On the basis of the hexagonal pore shape model, the experimental Q^3:Q^4 ratio yields a wall thickness of about 0.95 nm for MCM-41 silica, corresponding to the width of ca. four silica tetrahedra. The arrangement of Q^3 groups at the silica surfaces was analyzed using postsynthesis surface functionalization. It was found that the number of covalent bonds to the surface formed by the functional reagents is affected by the surface morphology. It is concluded that for high-quality MCM-41 silicas the distance between neighboring surface silanol groups is greater than 0.5 nm. As a result, di- and tripodical reagents like $(CH_3)_2Si(OH)_2$ and $CH_3Si(OH)_3$ can form only one covalent bond to the surface. The residual hydroxyl groups of surface-bonded functional reagents either remain free or interact with other reagent molecules. Accordingly, the number of surface silanol groups at a given MCM-41 or SBA-15 silica may not decrease but increase after treatment with $CH_3Si(OH)_3$ reagent. On the other hand, nearly all surface silanol groups could be functionalized when $HN(Si(CH_3)_3)_2$ was used.

Introduction

In recent years, novel porous materials that are periodically structured on the mesoscopic length scale were synthesized.[1−3] These periodic mesoporous materials opened up intriguing new application possibilities in catalysis,[4] drug delivery, size selective molecular separation,[5] and other fields, which in turn have triggered several studies of the dynamics of guest molecules in these materials.[6]

One of the intriguing questions concerning periodic mesoporous silica materials is the atomic-scale structure of their pore walls. At a mesoscopic level, the structure of these materials has been studied extensively by X-ray and neutron diffraction, as well as transmission and scanning electron microscopy.[7−12] MCM-41 and SBA-15 types of mesoporous silicas (space group *P*6*mm*) constitute a two-dimensionally (2D) ordered array of pores of uniform size disposed parallel to each other and separated by thin walls. These materials have a pore diameter in the range from 2 nm to more than 10 nm and a wall thickness of typically 25−50% of the pore diameter.[9] The concentration of silanol groups at the surface of the pore walls was found to be about 2.9 nm^{-2} for MCM-41 and 3.7 nm^{-2} for SBA-15 silicas.[13,14] The porosity of SBA-15 silica was characterized by ^{129}Xe NMR spectroscopy.[15] However, more detailed information about the structure of the pore walls and inner surfaces of these materials is lacking. These details are not only of academic interest but also of importance for applications of these materials as catalysts and host materials.

Current progress in material structure modeling is not sufficient to produce a representative atomic-scale structure of periodic mesoporous silica materials. One of the obstacles is that one does not have a reliable initial guess structure. Crystalline structures (β-tridymite, β-cristobalite, or edingtonite) do not satisfy the condition for the surface silanol densities.[13−19] More flexible molecular dynamics simulations are typically constrained to a total simulation time of nanoseconds. As a result, they do not provide sufficient time for the initial guess structure to relax to the energetically most favorable structure. Further progress in the modeling of these amorphous silica structures depends on more detailed information about the distribution of the silanol groups at the inner surfaces and the wall structure.

* Corresponding authors. I.G.S: phone, (+49) 30-838-53615; fax, (+49) 30-838-55310; e-mail, shender@chemie.fu-berlin.de. H.-H.L: e-mail, limbach@chemie.fu-berlin.de.
† Freie Universität Berlin.
‡ St. Petersburg State University.
§ Technische Universität Berlin.
‖ Universität Jena.

10.1021/jp073682m CCC: $37.00
Published on Web 10/04/2007

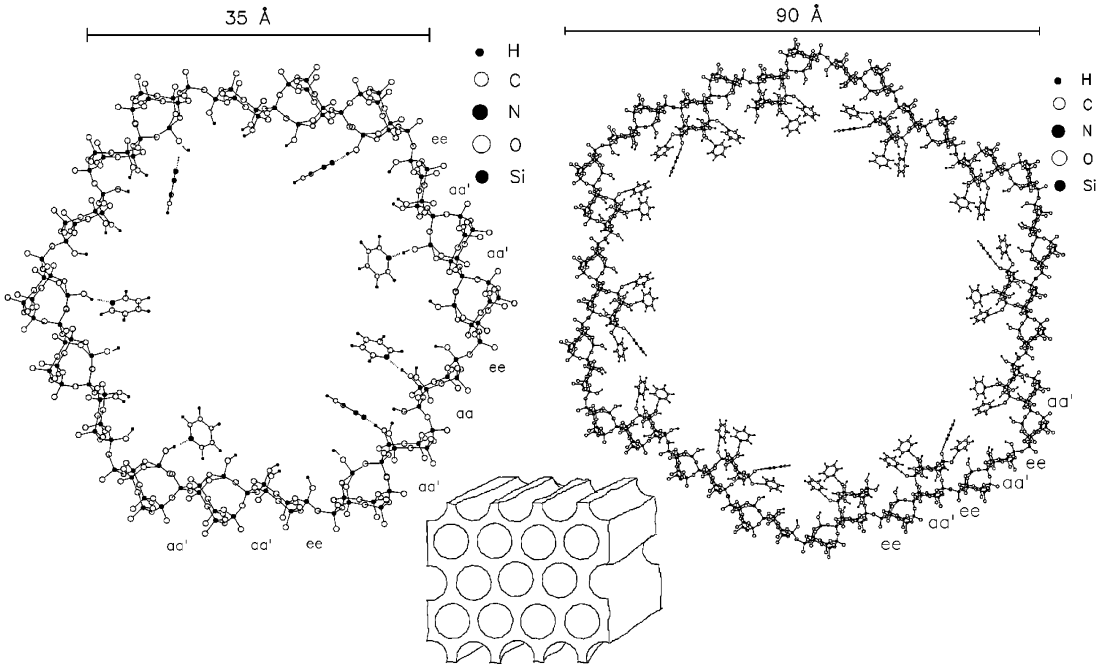

Figure 1. Atomic-scale models of the pore wall of MCM-41 (left) and SBA-15 (right) silica constructed using fragments derived from the unit cell of tridymite. The models exhibit experimental features of the respective silica.

Recently, some of the present authors developed an experimental procedure to examine the roughness of the inner surfaces of porous silica and the accessibility of the silanol groups to guests and to quantify the density of these silanol groups.[13] This procedure was based on a specific dependence of the ^{15}N chemical shift of hydrogen-bonded pyridines on the length of the corresponding N···H distance.[20] The most important conclusion to be drawn from that study was that the inner surfaces of high-quality MCM-41 samples were smooth on an atomic scale, while the surfaces of SBA-15 silica were rough, as depicted schematically in Figure 1. A 2D structure model of the inner surface of MCM-41 was proposed on the basis of the simplifying assumption that the chemical structure may be simulated using low-molecular-weight fragments derived from the unit cell of tridymite. In this way it was possible to construct an idealized silica surface having about three silanol groups per nm^2, in agreement with the experimental value for MCM-41 silica. The rough surface of SBA-15 pore walls could be simulated by decorating this idealized surface with additional single tridymite fragments as "surface defects", which leads to a higher density of the surface silanol groups, as observed experimentally (see Figure 1). Irrespective of whether the proposed structural motifs can serve as starting structures for more detailed simulations, they help to formulate a check list of criteria that have to be met by any realistic model: (i) the surface density of silanol groups; (ii) the distribution of these groups (uniform or nonuniform); and (iii) the relative amounts of different silicon species in the material, expressed by the ratio Q^2:Q^3:Q^4. For MCM-41, the surface density of the silanol groups (about 3 OH/nm^2) was known from the earlier study.[13] The structural model of Figure 1 implies a nonuniform distribution of the silanol groups at the inner surfaces. However, this prediction remained experimentally untested so far. Once the concentration of surface silanol groups at the pore wall is known, the ratio of Q^3 and Q^4 silica groups of "ideal" MCM-41 silica can be estimated from the pore diameter D and lattice parameter a_0 of the pore lattice (see Figure 5). Ideal MCM-41 silica does not contain Q^2 species, but these species will be present when the surface has defects. We are not aware of any reliable published data of the Q^2:Q^3:Q^4 ratio for MCM-41 silica.

A motivation for the present work has been to specify a set of criteria that must be met by realistic structural models of MCM-41 type materials. For this purpose, two types of measurements were necessary: (i) determination of the Q^2:Q^3 and Q^3:Q^4 ratio for MCM-41 and SBA-15 silica and (ii) study of the arrangement of Q^3 silicon via postsynthesis surface functionalization. As a prerequisite for point i, it was necessary to define experimental conditions for the ^{29}Si NMR measurements at which the integrated intensities of the Q^3 and Q^4 silicon signals can be compared in a quantitative manner. For point ii, surfaces of the silica samples were functionalized using reagents having one, two, or three reactive groups. For each reagent, the ratio of the numbers of single-, double-, and triple surface-bound species was obtained. This ratio provides qualitative information about the arrangement of the surface silanol groups. Finally, a list of general criteria suitable to select a model of mesoporous silica was specified and the previously proposed models were tested.

Experimental Section

Materials. The SBA-15 samples were prepared according to the prescription of Zhao et al.[21] employing a technical-grade PEO−PPO−PEO triblock copolymer (Pluronic P123, BASF Corp., Mount Olive, NJ) as the templating agent. A 4 wt % aqueous solution of P123 was treated with aqueous H_2SO_4 to reach a pH of ca. 1.5. Tetraethoxysilane (TEOS) was added to this solution with stirring at 40 °C. The precipitated product was kept in the reaction solution at 35 °C for 24 h and then at 100 °C for another 24 h. After rinsing with pure water and drying at 105 °C, the powder was heated to 180 °C in air for 4 h, to remove most of the polymer template, and finally calcinated at 550 °C under air flow.

The MCM-41 samples were synthesized following the procedure of Grün et al.[22] in aqueous ammonia solutions, using C_{10}- and C_{16}-trimethylammonium bromide as template molecules and again TEOS as the silica precursor. The precipitated

TABLE 1: Characterization of the Silica Materials by Nitrogen Adsorption (77 K) and X-ray Diffraction: Pore Condensation Pressure, $(p/p_0)_{pc}$; Cumulative Specific Surface Area, a_{BET}; Pore Volume at the Plateau Value of Adsorption Isotherm, v_p; Hydraulic Pore Diameter, $D_{hydr} = 4v_p/a_{BET}$; Pore Diameter, D; and Unit Cell Dimension, a_0

sample	silica material	$(p/p_0)_{pc}$	a_{BET}, $m^2\ g^{-1}$	v_p, $cm^3\ g^{-1}$	D_{hydr}, nm	D, nm	a_0, nm
M1	MCM-41	0.133	665	0.36	2.2	2.6	3.50
M2	MCM-41	0.358	1000	0.96	3.8	3.9	4.67
S1	SBA-15	0.758	815	1.04	5.1	8.9	11.64
S2	SBA-15	0.763	725	0.82	4.5	9.0	11.81

products were heat-treated, dried, and calcinated in a similar way as the SBA-15. Details of the synthesis are given elsewhere.[23]

The porosity and pore structure of the silica materials were characterized by nitrogen adsorption and small-angle XRD. Results for the samples **M1**, **M2**, **S1**, and **S2** are summarized in Table 1. The values of the cumulative specific surface area (a_{BET}) and the cumulative pore volume (v_p) were obtained from the flat plateau region of the isotherm above pore condensation, using the DFT pore size analysis method.[24] The pore diameter (D) was derived from the pore condensation pressure [$(p/p_0)_{pc}$] by the improved Kruk−Jaroniec−Sayari relation.[25] For ideal cylindrical pores, the pore diameter is given by the hydraulic diameter $D_{hydr} = 4v_p/a_{BET}$. Table 1 shows that $D \approx D_{hydr}$ holds true for the two MCM-41 materials but not for the SBA-15 materials, indicating that SBA-15 has a more complex pore structure than MCM-41. The lattice parameter of the 2D hexagonal pore lattice was calculated from the position of the (10) Bragg reflection as $a_0 = 4\pi/(\sqrt{3}q_{10})$. Experimental details are given elsewhere.[23]

NMR Measurements. All ^{15}N and ^{29}Si NMR measurements were performed on a Bruker MSL−300 instrument, operating at 7 T, equipped with a Chemagnetics-Varian variable-temperature 6 mm pencil CPMAS probe. The ^{29}Si spectra were recorded by employing a $\pi/12$ pulse-sequence under magic angle spinning (MAS, 6000 Hz) conditions and the $\{^1H\}-^{29}Si$ CPMAS experiment using a relatively long cross polarization (CP) contact time of 8 ms. This long CP time ensures sufficient polarization transfer to all different species of silica, i.e., Q^2, Q^3, and Q^4. The ^{29}Si chemical shifts are referenced to liquid TMS. The low-temperature ^{15}N MAS measurements at 120 K were performed by employing the $\{^1H\}-^{15}N$ CPMAS technique with a cross-polarization contact time of 5 ms. All ^{15}N chemical shift values are referenced to solid $^{15}NH_4Cl$. In this scale, pyridine resonates at 275 ppm and the protonated pyridinium below 170 ppm.[20,26] Typical 90°-pulse length was 3.5 μs for ^1H, 4.5 μs for ^{15}N, and 12 μs for ^{29}Si.

Sample Preparation. *Modification of SBA-15 with Hexamethyldisilazane ($HN(Si(CH_3)_3)_2$, HMDS) and Dichlorodimethylsilane ($(CH_3)_2SiCl_2$, DCDMS).* Both modifications were carried out by gas-phase reaction. SBA-15 (1.0 g) was put in a small flask, which was placed unsealed in the glass flask of the equipment. At 120 °C it was then evacuated for several hours to a pressure of 10^{-2} mbar to remove adsorbed water from the pores. Afterward, the corresponding reagent (hexamethyldisilazane or dichlorodimethylsilane, both from Fluka Co.) was dropped into the reaction chamber, where it condensed in the mesopores of the silica material. In case of HMDS, the flask was kept for 1 day at room temperature; in case of DCDMS, it was kept for 1 day at 100 °C. After that, the reagent that has not reacted was exhausted at 120 °C and 10^{-2} mbar via N_2-cryotrap.

TABLE 2: Overview and Abbreviations of the Unmodified and Modified Samples Used in This Work

sample	silica material	modified with
DM	DMDMS[a]	HCl[c]
TM	MTMS[b]	HCl[c]
S-HMDS	SBA-15	HMDS[d]
S-DC	SBA-15	DCDMS[e]
M-DM	MCM-41	DMDMS[a]
S-DM	SBA-15	DMDMS[a]
M-TM	MCM-41	MTMS[b]
S-TM	SBA-15	MTMS[b]

[a] Dimethyldimethoxysilane, $(CH_3)_2Si(OCH_3)_2$. [b] Methyltrimethoxysilane, $CH_3Si(OCH_3)_3$. [c] Hydrolyzed with an excess of 0.1 M HCl. [d] Hexamethyldisilazane, $HN(Si(CH_3)_3)_2$. [e] Dichlorodimethylsilane, $(CH_3)_2SiCl_2$.

Hydrolysis and Condensation of Pure Dimethyldimethoxysilane ($(CH_3)_2Si(OCH_3)_2$, DMDMS) and Methyltrimethoxysilane ($(CH_3)Si(OCH_3)_3$, MTMS). The reaction was performed by using an excess of two molecules of water per methoxy group under acidic conditions. The mixing ratios were 2.0 mL of DMDMS (14.6 mmol) with 1.0 mL (58.4 mmol) of 0.1 M HCl aqueous solution, and 2.0 mL of MTMS (14.1 mmol) with 1.5 mL (84.6 mmol) of 0.1 M HCl aqueous solution. After 2 days of stirring at room temperature, the condensation of the DMDMS mixture resulted in a clear, slightly viscous liquid and, in case of the MTMS mixture, in a cloudy gel-like substance.

Modification of MCM-41 and SBA-15 with Dimethyldimethoxysilane ($(CH_3)_2Si(OCH_3)_2$, DMDMS) and Methyltrimethoxysilane ($(CH_3)Si(OCH_3)_3$, MTMS). MCM-41 and SBA-15 (0.5 g each) were each suspended in dry toluene in N_2-atmosphere. Then the reagents DMDMS or MTMS (from Sigma Aldrich Co.) were added in excess under stirring slowly through a dropping funnel in the suspension flask. The mixture was then heated to 80 °C under reflux for 24 h. After the reaction the solid material was vacuum-filtrated and washed with 25 mL of each toluene and chloroform. Afterward, the solid was dried in a drying closet at 80 °C.

Results

In this section, we report the results of our solid-state NMR measurements. The samples were characterized by two types of experiments: (i) ^{29}Si MAS NMR of original silicas to obtain the Q^3:Q^4 ratio and (ii) ^{29}Si CPMAS NMR of functionalized silicas to inspect the arrangement of the surface silanol groups. We recall that the direct ^{29}Si NMR is extremely time-consuming, due to quite a long T_1 relaxation time. This problem can be overcome by employing a conventional ^{29}Si NMR CP technique. However, in general, the relative signal intensities in the latter case depend in a complicated way on the dipolar $^{29}Si-^1H$ couplings. Nevertheless, when the contact time is sufficiently long, the relative signal intensities can be compared for chemically similar species, giving an approximate ratio only.

Description and properties of silica materials used in this work are given in Tables 1 and 2.

^{29}Si MAS NMR Measurements of Original Silicas. The typical experimental spectra obtained for mesoporous silicas are presented in Figure 2. Four silica samples, two of MCM-41 type (**M1**, **M2**) and two of SBA-15 type (**S1**, **S2**), were analyzed in this work (see Table 1). The relative signal intensities obtained by signal deconvolution are listed in Table 3. Since both Q^2 and Q^3 species are carrying hydroxyl groups, their relative amounts can be estimated from the corresponding ^{29}Si CPMAS NMR spectra. MCM-41 silica samples contained much less Q^2 species as compared to SBA-15 ones. However, in all cases

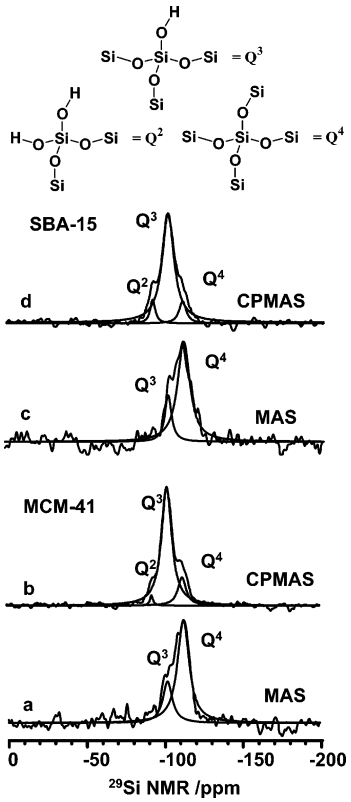

Figure 2. Experimental NMR spectra of ordered mesoporous silica materials (samples **M1** and **S1**) and their deconvolution: ^{29}Si MAS NMR of MCM-41 (a) and SBA-15 (c) and ^{29}Si CPMAS NMR of MCM-41(b) and SBA-15 (d).

TABLE 3: Relative Intensities of NMR Signals Corresponding to Different Silicon Species of the Ordered Mesoporous Silica Samples Studied in This Work

sample	Q^2:Q^3 (CPMAS)	Q^3:Q^4 (MAS)	sample	Q^2:Q^3 (CPMAS)	Q^3:Q^4 (MAS)
M1	3:100	32:100	**S1**	9:100	26:100
M2	1:100	35:100	**S2**	9:100	23:100

the Q^2:Q^3 ratios were small numbers, indicating that the Q^2 species result from structural defects rather than constituent structural units (see Table 3). The relative intensity of Q^4 species was strongly suppressed in these spectra by the cross-polarization procedure due to the absence of directly bonded hydroxyl groups. This problem was solved by combining a short $\pi/12$ pulse with a long relaxation delay of 240 s. The suitable relaxation delay was determined in a set of experiments by increasing the pulse repetition time in 60 s steps at the $\pi/12$ pulse length until the Q^3:Q^4 ratio became constant. For the two MCM-41 samples, the experiments gave a Q^3:Q^4 ratio of about 1:3. For the two SBA-15 samples, which have wider pores and a significantly greater wall thickness than MCM-41, the experiments gave a Q^3:Q^4 ratio close to 1:4.

^{29}Si CPMAS NMR Measurements of Functionalized Silica. Many potential applications of ordered mesoporous silica result from the surface silanol groups at the pore walls. The proton donor ability of the surface hydroxyls is similar to that of acids exhibiting a pK_a of about 4 in water.[13] Thus, the surface of pure silica is slightly acidic. The chemical activity of the surface can be selectively modified via the grafting method or templated sol−gel technology, leading to novel hybrid materials.[27−30] The simplest way to convert the weakly acidic surface of pure silica into a hydrophobic one is to coat it with hexamethyldisilazane ($HN(Si(CH_3)_3)_2$, HMDS). In this case, the functionalization reagent contains the only reactive group that can interact with the surface silanols to form the Si−O−Si covalent bond. Typical experimental spectra obtained for the original (**S1**) and functionalized (**S-HMDS**) SBA-15 silicas are presented in Figure 3. The level of the modification could be roughly estimated from the ^{29}Si CPMAS NMR spectrum of the functionalized silica by analyzing the reduction of the corresponding Q^3 peak [Figure 3a,b (left)]. If needed, the same could be done quantitatively using ^{15}N-labeled pyridine as described in detail in an earlier paper.[13] However, for the moment, it is sufficient to note that surface modification with HMDS causes a strong reduction of the amount of pyridine bound to the surface hydroxyl groups via hydrogen bonds [Figure 3a,b (right)]. It appears that HMDS causes a nearly quantitative functionalization of the surface. In contrast, the efficiency of the functionalization was strongly decreased when halogenated alkylsilanes, namely dichlorodimethylsilane ($(CH_3)_2SiCl_2$, DCDMS), were used, (sample **S-DC**, Figure 3c). Again, the ^{29}Si spectrum indicated that the functionalization went at the expense of the original Q^3 species. As a result, the ratio of the Q^3:Q^4 intensities for this sample was smaller than for the original silica [Figure 3a,c (left)]. In contrast, the corresponding ^{15}N spectra did not display a reduction of the available hydroxyl groups [Figure 3a,c (right)]. This finding indicated that some of the reactive groups of such reagents did not form covalent bonds to the surface but were only hydrolyzed. Since the hydrolyzation is the mandatory preliminary step of surface functionalization, we have to conclude that not all hydrolyzed groups were able to meet surface hydroxyl groups to form covalent bonds. This fact has been employed to analyze the arrangement of the surface hydroxyl groups.

In order to simplify the comparison between HMDS and reagents having two or three reactive groups, we studied silica samples modified by the simplest possible reagents, namely dimethyldimethoxysilane ($(CH_3)_2Si(OCH_3)_2$, DMDMS) and methyltrimethoxysilane ($CH_3Si(OCH_3)_3$, MTMS). Figure 4 shows ^{29}Si NMR spectra of these reagents after hydrolysis and condensation as well as spectra of functionalized silica materials (samples **DM**, **M-DM**, **S-DM**, and **TM**, **M-TM**, **S-TM**). The spectra of the functionalized materials were obtained using the cross-polarization transfer technique, so the relative intensities of different peaks of the same spectrum may not precisely coincide with the relative concentration of the corresponding species. On the other hand, a long contact time was used and each silicon atom carried at least one methyl group that minimized the difference. Thus, the relative intensities of these peaks could be mutually compared and used in order to estimate the relative concentrations of the species. The hydrolysis of pure DMDMS in 0.1 M HCl aqueous solution (**DM**) resulted mostly in the condensation. The residual amount of silicon atoms carrying one hydroxyl group, D^1 species, was small (Figure 4a). In contrast, the D^1:D^2 ratio was close to 2 when this reagent was used to modify MCM-41 silica (**M-DM**) and about 1 for SBA-15 silica (**S-DM**) (Figure 4b,c). The condensation of pure MTMS in 0.1 M HCl aqueous solution (**TM**) was less efficient. About 20% of the silicon atoms were still carrying one hydroxyl group, T^2 species (Figure 4d). On MCM-41, only about 60% of the reagent molecules were forming two covalent bonds to the surface and almost no molecules were forming three bonds (**M-TM**) (Figure 4e). The T^1:T^2:T^3 ratio on the surface of SBA-15 was about 1:10:4 (**S-TM**) (Figure 4f). The resulting T^1:T^2:T^3 ratios are summarized in Table 4.

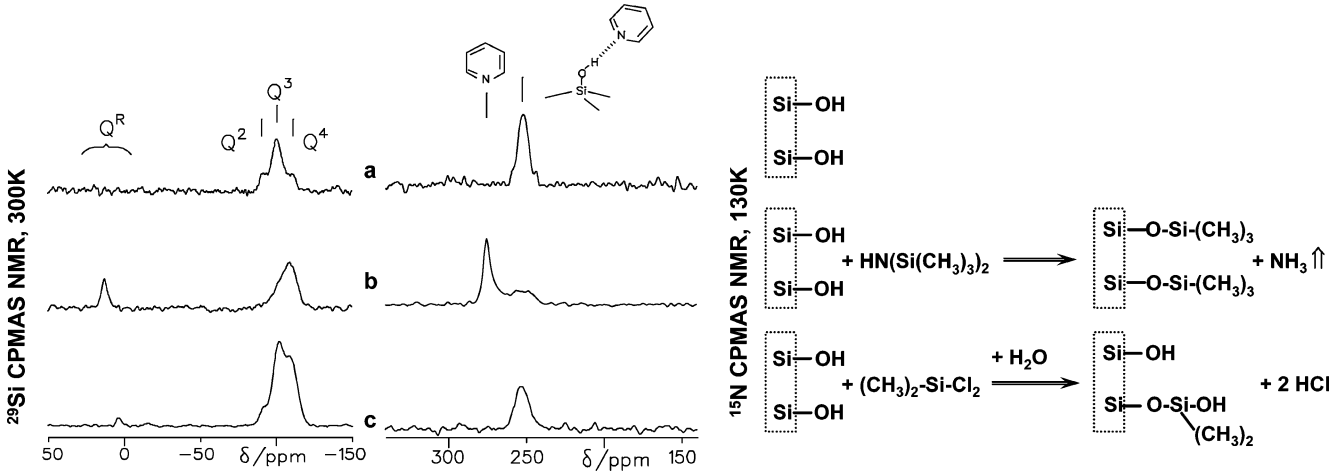

Figure 3. (Left) ^{29}Si CPMAS NMR of original (sample **S1**) (a) and functionalized (b, c) SBA-15 silica. (Right) ^{15}N CPMAS NMR at 130 K of the same samples loaded with an equal amount of ^{15}N-pyridine. The functionalization reagents were $(HN(Si(CH_3)_3)_2$, for sample **S-HMDS** (b), and $(CH_3)_2SiCl_2$, for sample **S-DC** (c). The chemical structures of the surfaces before and after functionalization are shown schematically. Q^R being the surface-bound functional groups.

Discussion

The main results of the experiments described above can be summarized as follows. ^{29}Si MAS NMR measurements of original silicas showed different Q^3:Q^4 ratios for MCM-41 and SBA-15 silicas. Namely, this ratio was about 1:3 for MCM-41 but about 1:4 for the SBA-15 samples. ^{29}Si CPMAS NMR measurements of functionalized silicas indicated that the number of covalent bonds formed by guest reagents depended on the surface roughness. The experimental data could be interpreted as that the surface of MCM-41 did not contain neighboring silanol groups that would be able to form covalent bonds with the same molecule of $(CH_3)_2Si(OH)_2$ or $CH_3Si(OH)_3$ type. In contrast, such molecules could be multiply bonded to the silica surface in the presence of surface defects, for example, on the surface of SBA-15.

Q^3:Q^4 from the Unit Cell Dimensions. For MCM-41 silicas, the number of Q^3- and Q^4-type entities per unit length of the 2D unit cell can be estimated from the volume of the silica matrix (V_m) and the surface area of the pore wall (A_p) in this unit cell if the number of silanol groups per unit area is known. V_m is obtained from the volume of the unit cell ($V = \sqrt{3}a_0^2/2$ per unit length, where a_0 is the lattice parameter) and the respective volume of the pore (V_p) as $V_m = V - V_p$. The total number of silica entities in this volume, N, is calculated as $N = V_m/v_{SiO_2}$, where v_{SiO_2} is the mean volume per silica entity, $v_{SiO_2} = M_{SiO_2}/(N_A\rho_{SiO_2})$, with M_{SiO_2} being the molar mass, ρ_{SiO_2} being the density of SiO_2, and N_A being the Avogadro's number. The number of Q^3 entities (silanol groups) is given by $N_3 = n_{SiOH}A_p$, where n_{SiOH} is the surface density of silanol groups. Finally, the number of Q^4 entities is obtained as $N_4 = N - N_3$. For the present MCM-41 and SBA-15 materials, the ratio $N_3/N_4 = Q^3$:Q^4 was estimated from the known values of the lattice parameter a_0, the pore radius $R = D/2$ (Table 1), and the surface density of silanol groups ($n_{SiOH} = 3.0$ nm^{-2} for MCM-41 and $n_{SiOH} = 3.7$ nm^{-2} for SBA-15),[13] using $\rho_{SiO_2} = 2.20$ g cm^{-3}. Two pore geometry models, viz., pores of circular and hexagonal cross section, were tested (Figure 5). For pores of circular cross section, V_m and A_p are given by

$$V_m = \left(\frac{\sqrt{3}}{2}a_0^2 - \pi R^2\right), A_p = 2\pi R$$

and for pores of hexagonal cross section, one finds

$$V_m = \sqrt{3}(a_0 - d/2)d, A_p = 2\sqrt{3}(a_0 - d)$$

where d is the wall thickness of the honeycomb structure. In the calculations, we set $d = a_0 - D$, i.e., the same wall thickness as for pores of circular cross section (Figure 5). Results of this analysis are given in Table 5. For the two MCM-41 samples (**M1** and **M2**), the estimated values of Q^3:Q^4 are in reasonable agreement with the experimental Q^3:Q^4 values. For both samples, the Q^3:Q^4 ratio resulting from the circular cross section model is somewhat lower than the experimental value, while the Q^3:Q^4 ratio resulting for the hexagonal cross section model is somewhat higher than the experimental value, implying that the pore shape of the MCM-41 materials is intermediate between hexagonal and circular. This finding is consistent with results of X-ray structural modeling of a MCM-41 material similar to our sample **M2**.[8] Incidentally, the above model may also be used to calculate the thickness of the pore walls by using the experimental Q^3:Q^4 value as an input. The hexagonal pore shape model yields a wall thickness of 0.95 nm for both **M1** and **M2**, i.e., somewhat greater than the values resulting from the relation $d = a_0 - D$ (Table 5). This wall thickness corresponds roughly to the width of four silicate tetrahedra.[31]

For the SBA-15 samples (**S1** and **S2**), the above model strongly underestimates the experimental Q^3:Q^4 ratio (see Table 5), indicating that in these materials the surface area of the pore walls is significantly greater than that of idealized model pores of circular or hexagonal cross section. This finding is consistent with the conclusions of the earlier NMR study,[13] as well as X-ray[32−34] and neutron[35] small-angle diffraction studies, which point to the existence of a microporous corona around the cylindrical pores (or a highly corrugated surface of the pore walls) of SBA-15 samples. These structural features are not taken into account in the above simple model.

Modeling of the Interpore Walls of Idealized Mesoporous Silica. In our earlier work,[13] atomic-scale models of the inner surfaces of MCM-41 and SBA-15 silica were proposed (see Figure 1) that conform to the experimental values of the density of surface silanol groups. The models were compared to other possible models based on the unit cells of tridymite[36] and edingtonite.[19] Here we examine whether these models are consistent with the experimental Q^3:Q^4 ratio obtained in this work.

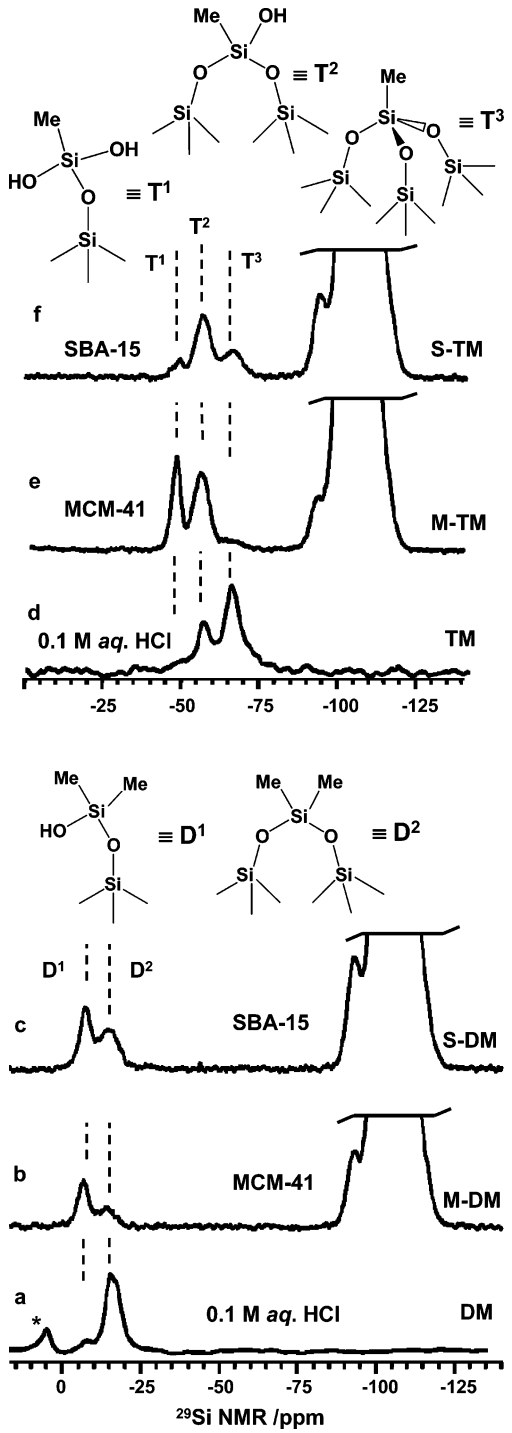

Figure 4. (Bottom) Silica samples functionalized using DMDMS as reagent: ^{29}Si NMR of hydrolyzed dimethyldimethoxysilane (DMDMS), sample **DM** (a), and ^{29}Si CPMAS NMR of MCM-41, sample **M-DM** (b), and SBA-15, sample **S-DM** (c). (Top) Silica samples functionalized using MTMS as reagent: ^{29}Si NMR of hydrolyzed methyltrimethoxysilane (MTMS), sample **TM** (d), and ^{29}Si CPMAS NMR of MCM-41, sample **M-TM** (e), and SBA-15, sample **S-TM** (f).

Figure 6 shows fragments from the unit cells of (a) tridymite, (b) edingtonite, and (c) a fictitious unit cell selectively constructed from differently bonded tridymite fragments. The large circles represent Q^4 species, while the triangles carrying small circles represent surface Q^3 species. The unit layers forming the pore walls are represented as differently shaded areas. Since the distance between nearest-neighbor Si atom layers of silica is about 0.24 nm, the density of surface silanol groups is expected to be approximately 4.5 nm^{-2} (tridymite), 2.2 nm^{-2} (edingtonite), and 3.0 nm^{-2} for the MCM-41 model (c). The last of these values agrees with the experimental value for MCM-41 silicas. Figure 6 also gives the Q^3:Q^4 ratios for these fragments, which are 1:1 for tridymite, 1:4 for edingtonite, and 1:3 for MCM-41 silica. Accordingly, the edingtonite unit cell (Figure 6b) cannot serve as a building block for MCM-41 silica, as it conforms neither to the experimental value of the surface density of silanol groups nor to the experimental Q^3:Q^4 ratio. A combination of four unit layers of tridymite (Figure 6a) is consistent with the observed Q^3:Q^4 ratio, but not with the surface density of silanol groups and the experimental wall thickness of less than 1 nm. For the structural fragment of Figure 6c, the Q^3:Q^4 ratio is 1:3, and a bilayer formed by two such fragments represents a structure that meets all experimental requirements, when taking into account that the resulting surface is not planar. The mean thickness of about 1.0 nm of such a bilayer is close to the experimental wall thickness of MCM-41 silica. However, it must be emphasized that the mutual agreement of the parameters for this fictitious atomic-scale structure and of the idealized mesoscale model of MCM-41 does not mean that these atomic-scale structural fragments reproduce the true structure of the pore walls of MCM-41. In particular, the properties of the 3D structure formed by this unit cell have to be checked. Nevertheless, the formal agreement suggests that tridymite fragments can be used as building blocks to construct the initial guess model suitable for structural refinement.

TABLE 4: Relative Intensities of NMR Signals Corresponding to Surface Functional Groups of Different Podality

sample	D^1:D^2	T^1:T^2:T^3
DM	5:100	
TM		55:100:354
M-DM	223:100	
S-DM	91:100	
M-TM		62:100:−
S-TM		7:100:38

We emphasize that the present model cannot account for the wall structure of SBA-15, due to its more complex structure as compared to MCM-41. Specifically, SBA-15 is characterized by a significantly greater wall thickness (see Table 5), and the pores are surrounded by a microporous "corona" of lower density than for bulk silica.[32−34] Qualitatively, the greater wall thickness of SBA-15 is reflected by the lower values of the Q^3:Q^4 ratio, while the existence of a microporous corona (or of corrugated pore walls) is indicated by the fact that our simple mesoscopic model of cylindrical pores yields much too low values of the Q^3:Q^4 ratio (Table 5).

Arrangement of the Surface Silanol Groups. We showed that silica functionalization using HMDS ($HN(Si(CH_3)_3)_2$) as reagent allowed us to obtain a practically hydroxyl-free surface. This means that groups such as $Si(CH_3)_3$ being immobilized on the surface do not prevent functionalization of neighboring silanol groups. The diameter of the "cylinder" formed by the $Si(CH_3)_3$ group is about 0.5 nm. The mean surface density of the silanol groups is about 3 per nm^2. Thus, the mean distance between the neighboring silanol groups on such a surface is about 0.58 nm. These estimations do not allow us to conclude whether or not the silanol groups at the surface of ordered mesoporous silica are distributed uniformly. This question might be answered by analyzing the rotational dynamics of the immobilized functional groups. The estimations predict only the lower limit for the distance between the neighboring silanol groups on the idealized surface. The latter indicates that any functionalization reagent of the $(CH_3)_{4-n}Si(OH)_n$ type could form only one covalent bond to the surface and the residual

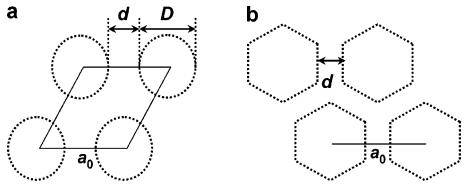

Figure 5. Sketch of idealized MCM-41 of circular (a) and hexagonal (b) cross sections of the pores.

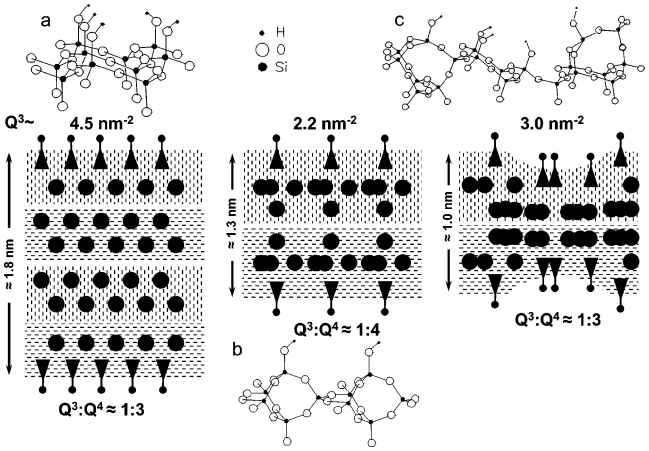

Figure 6. Scheme of the chemical structures of idealized surfaces and walls of tridymite (a), edingtonite (b), and model MCM-41 (c). The density of the surface silanol groups and the Q^3:Q^4 ratios are shown.

TABLE 5: Q^3:Q^4 Ratio of MCM-41 (M1 and M2) and SBA-15 (S1 and S2) Samples: Comparison of Experimental Q^3:Q^4 Ratio with Values Resulting from a Model of Ideal Mesopores of Circular or Hexagonal Cross Section Embedded in a Matrix of Uniform Density

				Q^3:Q^4		
sample	a_0, nm	d, nm	R, nm	exp.	circular	hexagonal
M1	3.50	0.9	1.30	0.32	0.27	0.35
M2	4.67	0.8	1.94	0.35	0.30	0.45
S1	11.64	2.7	4.47	0.26	0.09	0.12
S2	11.81	2.8	4.51	0.23	0.09	0.12

chemically active groups could be used only to form a new silica layer. This strategy was used by Ugliengo et al. in order to simulate the framework of edingtonite.[37]

A closer look at spectra of functionalized silica in Figure 4 shows that the half-widths of the NMR peaks corresponding to D^1 and D^2 or T^1 and T^2, T^3 species are different. The peaks corresponding to D^1 and T^1 species have only about half the width of those of D^2, T^2, and T^3. In contrast, the half-width of the NMR peaks corresponding to T^2 and T^3 species formed in aqueous solution after $CH_3Si(OMe)_3$ hydrolyzation was approximately the same as that of the D^1 and T^1 species on the silica surface. We ascribe this effect to inhomogeneous broadening due to some variations in the geometry of different D^2, T^2, and T^3 species bonded to the silica surface. These deviations could be caused either by the mutual bonding between the functional groups or their multiple bonding to the surface. Which of these two reasons plays the dominant role? We suppose that the answer is different for MCM-41 and SBA-15 silica. When the surface was functionalized using $CH_3Si(OMe)_3$ as the reagent, we did not observe T^3 bonded species on the MCM-41 surface. This finding is at variance with data reported in other studies.[38,39] However, it seems that in these studies the degree of functionalization was higher than for our samples. In this case, the formation of covalent bonds to further reagent molecules cannot be excluded. Indeed, the fact that the amount

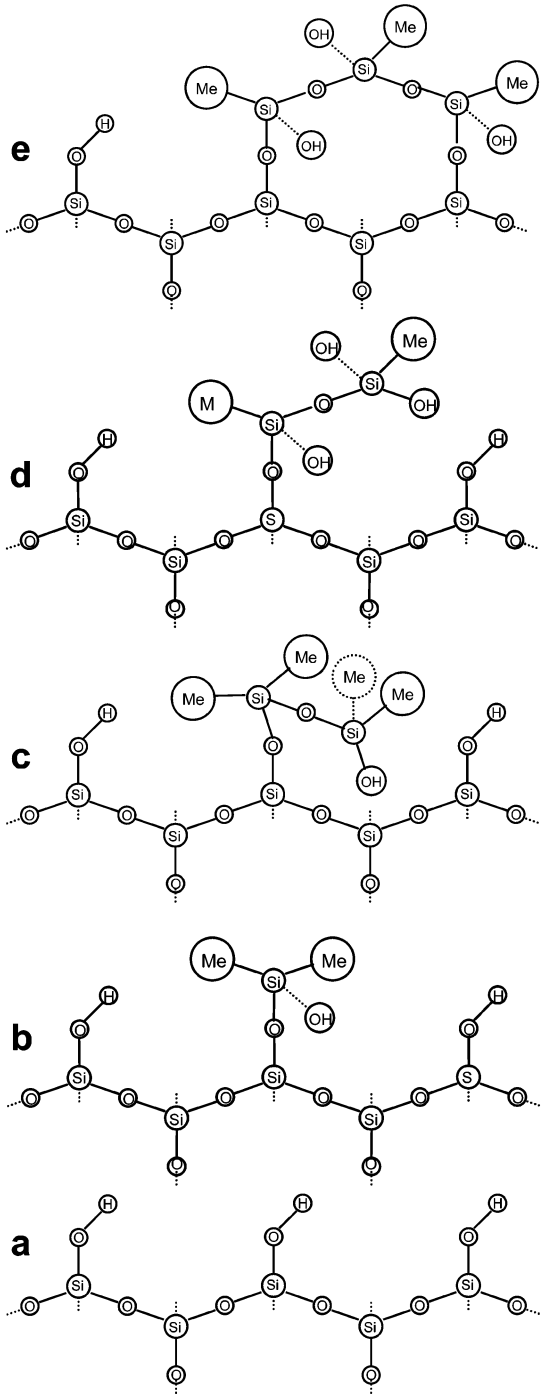

Figure 7. Cartoon of the surface structures of a silica before (a) and after its treatment with a small (b, d) and large (c, e) amount of $(CH_3)_2Si(OCH_3)_2$ and $CH_3Si(OCH_3)_3$ reagents.

of T^2 species on the MCM-41 surface was much higher than the amount of D^2 species, when $CH_3Si(OMe)_3$ reagent was used instead of $(CH_3)_2Si(OMe)_2$, could hardly be explained exclusively in terms of the covalent bonding to the surface. The hydroxyl group of the surface-bonded $(CH_3)_2Si(OH)$ species should be directed closer to the surface as compared to one of the hydroxyl groups of the surface-bonded $(CH_3)Si(OH)_2$ species, which must result in a better access of another reagent to the latter hydroxyl group. Thus, the surface of MCM-41 silica did not contain silanol groups that would be able to react with the same molecule of the $(CH_3)_{4-n}Si(OH)_n$ type reagent. If the formation of mutually bonded functional groups could be suppressed, such a surface would contain exclusively single

surface-bonded species. On the other hand, each surface silanol groups could carry the functional group. The amount of D^2, T^2, and T^3 species dramatically increases when the rough surface of SBA-15 was used instead of the quasi-ideal surface of MCM-41. It is not clear whether T^3 species observed on SBA-15 silica could be formed exclusively by the covalent bonding to the surface or by bonding to other functional groups as well. We assume that the latter case is more realistic.

In Figure 7 we summarize the above discussion in a pictorial way. Let us assume for simplicity a uniform arrangement of the silanol groups on the surface (Figure 7a). When the $(CH_3)_2Si(OMe)_2$ reagent is used to functionalize such a surface, it may form only one covalent bond, and the second active group is just converted to hydroxyl (Figure 7b). It is hard to imagine how this group could form the second covalent bond to the surface. Potentially, it might react with another reagent molecule (Figure 7c), but the experimental spectra indicated that such reaction was not very effective (Figure 4b). When the $CH_3Si(OMe)_3$ reagent is used, it may also form only one covalent bond to the surface, but at least one of the two residual free hydroxyl groups can be easily attacked by another reagent (Figure 7d). If no further reaction would take place, the T^1:T^2 ratio would be about 1:1. In contrast, the experimental data for this reagent on MCM-41 silica revealed a ratio of about 2:3 (Figure 4e). This may indicate that a third reagent molecule becomes involved, leading to the double surface bonded species (Figure 7e). The presence of surface defects will allow more complex structures with reduced numbers of unreacted hydroxyl groups, as was observed for SBA-15 silica.

Conclusion

The main goal of this study was to determine generic structural parameters of MCM-41 and SBA-15 type ordered mesoporous silicas that may be used as a checklist for atomic-scale structural models of this class of ordered mesoporous materials. For this purpose, we determined the Q^2:Q^3 and Q^3:Q^4 ratios and analyzed the arrangement of Q^3 silicon atoms at the inner surfaces of these silica materials. High-quality samples of MCM-41 and SBA-15 silica were used in this study. It was demonstrated that the Q^2:Q^3 ratio is quite small for all samples studied and that MCM-41 silica has a lower concentration of Q^2 species than SBA-15 silica. Previously it has been shown that the inner surfaces of high-quality MCM-41 silica show a significantly lower concentration of defects as compared to SBA-15 silica. The new findings support the view that the Q^2 species are due to structural defects of the silica surfaces. The Q^3:Q^4 ratio of MCM-41 samples is found to be about 1:3, while values close to 1:4 are found for the SBA-15 samples. One may expect that, similar to the surface structure, the pore walls of MCM-41 are more ordered than those of SBA-15 silica. Thus, the earlier finding[13] that the surface density of silanol groups is about three OH/nm^2 in high-quality MCM-41 silica is supplemented by the findings that high-quality MCM-41 samples contain a negligible number of Q^2 species and that the Q^3:Q^4 ratio is close to 1:3. Neither tridymite nor edingtonite meet both of these requirements, while the atomic-scale model of MCM-41 silica developed earlier by some of us[13] formally meets both conditions. Thus, the use of tridymite-based unit cell structures to construct a realistic model of MCM-41 silica must not be discarded. On the basis of the hexagonal pore shape model, the experimental Q^3:Q^4 ratio yields a wall thickness of about 0.95 nm for MCM-41 silica, corresponding roughly to the width of four silicate tetrahedra. This value agrees well with the experimental wall thickness of 0.8−0.9 nm as derived from the lattice spacing and pore size of the two MCM-41 samples.

The arrangement of Q^3 silicon on the silica surfaces was analyzed using postsynthesis surface functionalization. In particular, it is shown that $Si(CH_3)_3$ groups attached to the surface do not prevent reactions with the neighboring surface silanol groups. This fact indirectly indicates that the distance between neighboring surface silanol groups is greater than 0.4−0.5 nm. As a result, functional reagents of $(CH_3)_2Si(OH)_2$ and $CH_3Si(OH)_3$ type can form only one covalent bond to the surface of high-quality MCM-41 silica. The residual hydroxyl groups of the surface-bonded functional reagents either remain free or interact with other reagent molecules. On the other hand, it appears that multiple covalent binding to the surface is possible to some extent on the rough pore walls of SBA-15 silica, at least for the $CH_3Si(OH)_3$ reagent. In other words, the number of the covalent bonds formed by the functional reagents to the silica surface is affected by the surface morphology. The pore walls can be almost fully functionalized when HMDS is used as the functionalization agent. In contrast, at the same surface the number of silanol groups may even increase by functionalization under certain conditions when $CH_3Si(OH)_3$ is used as grafting agent.

Acknowledgment. We gratefully thank Russian Ministry of Education and Science (project RNP 2.1.1. 4139) and the Deutsche Forschungsgemeinschaft for financial support. This work was performed in the framework of Sonderforschungsbereich 448 (TP B1 and B2) and the Graduate School GK-788.

References and Notes

(1) Beck, J. S.; Vartuli, J. C.; Roth, W. J.; Leonowicz, M. E.; Kresge, C. T.; Schmitt, K. D.; Chu, C. T. W.; Olson, D. H.; Sheppard, E. W.; Mccullen, S. B.; Higgins, J. B.; Schlenker, J. L. *J. Am. Chem. Soc.* **1992**, *114*, 10834.

(2) Sayari, A.; Hamoudi, S. *Chem. Mater.* **2001**, *13*, 3151.

(3) Linssen, T.; Cassiers, K.; Cool, P.; Vansant, E. *Adv. Colloid Interface Sci.* **2003**, *103*, 121.

(4) (a) Morey, M. S.; Davidson, A.; Stucky, G. D. *J. Porous Mater.* **1998**, *5*, 195. (b) Chen, H. T.; Huh, S.; Wiench, J. W.; Pruski, M.; Lin, V. S. Y. *Abstr. Paper. Am. Chem. Soc.* **2005**, *229*, U983. (c) Chen, H. T.; Huh, S.; Wiench, J. W.; Pruski, M.; Lin, V. S. Y. *J. Am. Chem. Soc.* **2005**, *127*, 13305. (d) Wang, X. G.; Lin, K. S. K.; Chan, J. C. C.; Cheng, S. F. *J. Phys. Chem. B* **2005**, *109*, 1763.

(5) Vinu, A.; Hossain, K. Z.; Ariga, K. *J. Nanosci. Nanotechnol.* **2005**, *5*, 347.

(6) (a) Aksnes, D. W.; Gjerdaker, L. *J. Mol. Struct.* **1999**, *475*, 27. (b) Courivaud, F.; Hansen, E. W.; Kolboe, S.; Karlsson, A.; Stöcker, M. *Microporous Mesoporous Mater.* **2000**, *37*, 223. (c) Jobic, H. *Phys. Chem. Chem. Phys.* **1999**, *1*, 525. (d) Ladizhansky, V.; Hodes, G.; Vega, S. *J. Phys. Chem. B* **2000**, *104*, 1939. (e) Mel'nichenko, Y. B.; Schüller, J.; Richert, R.; Ewen, B.; Loong, C.-K. *J. Chem. Phys.* **1995**, *103*, 2016. (f) Gjerdaker, L.; Sorland, G. H.; Aksnes, D. W. *Microporous Mesoporous Mater.* **1999**, *32*, 305. (g) Hansen, E. W.; Schmidt, R.; Stöcker, M.; Akporiaye, D. *Microporous Mater.* **1995**, *5*, 143. (h) Gedat, E.; Schreiber, A.; Albrecht, J.; Shenderovich, I.; Findenegg, G.; Limbach, H.-H.; Buntkowsky, G. *J. Phys. Chem. B.* **2002**, *106*, 1977. (i) Valiullin, R.; Naumov, S.; Galvosas, P.; Kärger, J.; Woo, H.-J.; Porcheron, F.; Monson, P. A. *Nature* **2006**, *443*, 965. (j) Vyalikh, A.; Emmler, T.; Grünberg, B.; Xu, Y.; Shenderovich, I.; Findenegg, G. H.; Limbach, H.-H.; Buntkowsky, G. *Z. Phys. Chem.* **2007**, *221*, 155. (k) Vyalikh, A.; Emmler, T.; Gedat, E.; Shenderovich, I.; Findenegg, G. H.; Limbach, H.-H.; Buntkowsky, G. *Solid State NMR* **2005**, *28*, 117. (l) Masierak, W.; Emmler, T.; Gedat, E.; Schreiber, A.; Findenegg, G. H.; Buntkowsky, G. *J. Phys. Chem. B* **2004**, 18890.

(7) Taguchi, A.; Schüth, F. *Microporous Mesoporous Mater.* **2005**, *77*, 1.

(8) Solovyov, L. A.; Kirik, S. D.; Shmakov, A. N.; Romannikov, V. N. *Microporous Mesoporous Mater.* **2001**, *44*−*45*, 17.

(9) Sauer, J.; Marlow, F.; Schüth, F. *Phys. Chem. Chem. Phys.* **2001**, *3*, 5579.

(10) Ciesla, U.; Schüth, F. *Microporous Mesoporous Mater.* **1999**, *27*, 131.

(11) Schacht, S.; Janicke, M.; Schüth, F. *Microporous Mesoporous Mater.* **1998**, *22*, 485.

(12) Edler, K. J.; Reynolds, P. A.; White, J. W. *J. Phys. Chem. B* **1998**, *102*, 3676.
(13) Shenderovich, I. G.; Buntkowsky, G.; Schreiber, A.; Gedat, E.; Sharif, S.; Albrecht, J.; Golubev, N. S.; Findenegg, G. H.; Limbach, H.-H. *J. Phys. Chem. B* **2003**, *107*, 11924.
(14) Grünberg, B.; Emmler, T.; Gedat, E.; Shenderovich, I.; Findenegg, G. H.; Limbach, H. H.; Buntkowsky, G. *Chem. Eur. J.* **2004**, *10*, 5689.
(15) Nossov, A.; Haddad, E.; Guenneau, F.; Galarneau, A.; Di Renzo, F.; Fajula, F.; Gédéon, A. *J. Phys. Chem. B* **2003**, *107*, 12456.
(16) Zhuravlev, L. T. *Langmuir* **1987**, *3*, 316.
(17) Chuang, I.-S.; Maciel, G. E. *J. Phys. Chem. B* **1997**, *101*, 3052.
(18) Civalleri, B.; Casassa, S.; Garrone, E.; Pisani, C.; Ugliengo, P. *J. Phys. Chem. B* **1999**, *103*, 2165.
(19) Civalleri, B.; Ugliengo, P. *J. Phys. Chem. B* **2000**, *104*, 9491.
(20) Lorente, P.; Shenderovich, I. G.; Golubev, N. S.; Denisov, G. S.; Buntkowsky, G.; Limbach, H. H. *Magn. Reson. Chem.* **2001**, *39*, S18.
(21) Zhao, D.; Feng, J.; Huo, Q.; Melosh, N.; Fredrickson, G. H.; Chmelka, B. F.; Stucky, G. D. *Science* **1998**, *279*, 548.
(22) Grün, M.; Unger, K. K.; Matsumoto, A.; Tsutsumi, K. *COPS IV* **1997**, 81−89.
(23) Schreiber, A.; Ketelsen, I.; Findenegg, G. H. *Phys. Chem. Chem. Phys.* **2001**, *3*, 1185.
(24) Ravikovitch, P. I.; Neimark, A. V. *J. Phys. Chem. B* **2001**, *105*, 6817.
(25) Jaroniec, M.; Solovyov, L. A. *Langmuir* **2006**, *22*, 6757.
(26) Bismark, A.; Aranberri-Askargorta, I.; Lampke, T.; Wielage, B.; Stramboulis, A.; Shenderovich, I.; Limbach, H.-H. *Polym. Composites* **2002**, *23*, 872.
(27) Anwander, R. *Chem. Mater.* **2001**, *13*, 4419.
(28) Valkenberg, M. H.; Holderich, W. F. *Catal. Rev.* **2002**, *44*, 321.
(29) Hoffmann, F.; Cornelius, M.; Morell, J.; Fröba, M. *Angew. Chem., Int. Ed.* **2006**, *45*, 3251.
(30) Hoffmann, F.; Cornelius, M.; Morell, J.; Fröba, M. *J. Nanosci. Nanotechnol.* **2006**, *6*, 265.
(31) Solovyov, L. A.; Belousov, O. V.; Dinnebier, R. E.; Shmakov, A. N.; Kirik, S. D. *J. Phys. Chem. B* **2005**, *109*, 3233.
(32) Imperor-Clerc, M.; Davidson, P.; Davidson, A. *J. Am. Chem. Soc.* **2000**, *122*, 11925.
(33) Hofmann, T.; Wallacher, D.; Huber, P.; Birringer, R.; Knorr, K.; Schreiber, A.; Findenegg, G. H. *Phys. Rev. B* **2005**, *72*, 064122.
(34) Zickler, G. A.; Jähnert, S.; Wagermaier, W.; Funari, S. S.; Findenegg, G. H.; Paris, O. *Phys. Rev. B* **2006**, *73*, 184109.
(35) Schreiber, A.; Ketelsen, I.; Findenegg, G. H.; Hoinkis, E. *Stud. Surf. Sci. Catal.* **2006**, *160*, 17.
(36) Kihara, K. *Z. Kristallographie* **1980**, *152*, 95. Kihara, K. *Z. Kristallographie* **1981**, *157*, 93. CIF file 30795-ICSD from the Inorganic Cambridge Structure Database (ISCD).
(37) Ugliengo, P.; Civalleri, B.; Dovesi, R.; Zicovich-Wilson, C. M. *Phys. Chem. Chem. Phys.* **1999**, *1*, 545.
(38) Zhang, C.; Zhou, W.; Liu, S. *J. Phys. Chem. B* **2005**, *109*, 24319.
(39) Kumar, R.; Chen, H.-T.; Escoto, J. L. V.; Lin, V. S.-Y.; Priski, M. *Chem. Mater.* **2006**, *18*, 4319.